Published on 28 January 2016. Downloaded by Indian Institute of Technology Kanpur on 9/24/2021 8:03:59 AM.

Soft Matter

PAPER

View Article Online
View Journal | View Issue

Cite this: *Soft Matter*, 2016, 12, 3093

Molecular dynamics study of wetting behavior of grafted thermo-responsive PNIPAAm brushes

Debdip Bhandary,[a] Zuzana Benková,[bc] M. Natália D. S. Cordeiro[b] and Jayant K. Singh*[a]

Received 30th October 2015,
Accepted 25th January 2016

DOI: 10.1039/c5sm02684a

www.rsc.org/softmatter

In this work, the effect of temperature on the contact angle of a water droplet on grafted thermo-responsive poly-(*N*-isopropylacrylamide) (PNIPAAm) polymer brushes is studied using all-atom molecular dynamics simulations in the temperature range of 270–330 K. A shift from 55° to 65° in contact angle values is observed as the temperature increases from 300 K to 310 K, which is in line with the experimental reports. The behavior of a water droplet on PNIPAAm brushes is analyzed using hydrogen bond analysis, water diffusion, radial distribution functions, the potential of mean force, excess entropy and the second virial coefficient (B_2). The thermo-responsive behavior of PNIPAAm brushes, quantified using the excess entropy and B_2 of PNIPAAm–water and water–water interactions, is mainly governed by polymer–water interactions. In particular, the excess entropy and B_2 of PNIPAAm resulting from the PNIPAAm–water interactions are found to increase with increasing temperature. The dehydration of PNIPAAm brushes and the increase in the contact angle of water were confirmed to be entropy driven processes.

1. Introduction

Stimuli-responsive surfaces have become the area of interest for more than three decades. End-grafted polymers responsive to the changes in external conditions such as temperature, light, electric field, pH or ionic strength represent an easy and convenient way of manufacturing stimuli responsive surfaces. Poly(*N*-isopropylacrylamide) (PNIPAAm) is one of the most widely employed thermo-responsive polymers, with a large range of applications especially in the control of protein adsorption and cell attachment,[1,2] because of its lower critical solution temperature (LCST) of 32 °C, which is well within the physiological temperature range. PNIPAAm chains densely grafted onto surfaces may switch the film permeability and wetting characteristics.[3,4] Moreover, polymer films built up of PNIPAAm chains exhibit self-healing properties.[5,6] The presence of water plays a key role in the coil-to-globule transition of free PNIPAAm chains. PNIPAAm undergoes sharp conformational changes at the LCST, *i.e.*, it is water soluble below this temperature, and above this temperature it undergoes phase separation.

Several authors pointed out that the temperature-induced phase transition of free PNIPAAm chains in water originates from the alteration of hydrogen bonding between the amide groups of PNIPAAm chains and water molecules and reorganization of water molecules around hydrophobic isopropyl groups.[7–10] Many experimental as well as computational studies have dealt with the nature as well as the dynamics of hydrogen bonds.[11–14] For example, Graziano[13] studied the coil-to-globule transition for a diluted aqueous solution of free PNIPAAm employing differential scanning calorimetry. The coil to globule phase transition is characterized as an entropy driven endothermic process as the heat capacity of the coil state turned out to be higher than the heat capacity of the globule state. Deshmukh *et al.* performed molecular dynamics simulations of PNIPAAm hydrogels with a different density of crosslinking points slightly below, at and above the LCST to study the structural properties of these hydrogels as well as the dynamic behavior of water molecules.[15] The higher the crosslinking density, the less dramatic structural changes accompanied the coil-to-globule transition. The hydrogen bonds between the carboxyl oxygen and the water hydrogen were found to possess the longest lifetime regardless of the crosslinking density and temperature.

Because of the lateral repulsion among the polymer chains grafted onto a supporting substrate, the conformation and behavior of the chains considerably differ from the conformation and behavior of free polymer chains. The coil-to-globule transition of grafted PNIPAAm chains is not as sharp as it is for free PNIPAAm chains in the bulk phase and is also affected by the grafting density of PNIPAAm chains. A relatively wide interval of transition temperatures (~10–40 °C) for hydration–dehydration transition of the PNIPAAm brush film (grafted chain on a substrate)

[a] *Department of Chemical Engineering, Indian Institute of Technology Kanpur, UP, 208016, India. E-mail: jayantks@iitk.ac.in*
[b] *LAQV@REQUIMTE, Department of Chemistry and Biochemistry, University of Porto, 4169-007 Portugal*
[c] *Polymer Institute, Slovak Academy of Sciences, Dúbravská cesta 9, 845 41 Bratislava, Slovakia*

Published on 28 January 2016. Downloaded by Indian Institute of Technology Kanpur on 9/24/2021 8:03:59 AM.

was observed using surface plasmon resonance spectroscopy, while the contact angle measurements provided a sharp dehydration transition at 32 °C in agreement with the water solution of free PNIPAAm chains.[16] Thus the authors suggested that the outer region of the polymer film remained significantly solvated till the LCST of free PNIPAAm chains in aqueous solution (~32 °C), while the inner region of the film underwent dehydration over a broad temperature interval. Upon heating, the collapse of a PNIPAAm chain was completed at 41 °C. The swelling, induced by hydration, started at 37 °C. The data from the neutron reflectometry measurements pointed out that the dehydration is a phase transition process consisting of the formation of a distinct bilayer profile as the intermediate between the hydrated and dehydrated states.[17] In contrast, using the dynamic contact angle measurements, Takei *et al.* reported a transition temperature of 24 °C.[18] The expulsion of water molecules from the layer of grafted PNIPAAm chains appeared to be accompanied by a smooth cooperative conformational transition of the grafted layer.[16,17] Following the generalized theoretical analysis of Zhulina *et al.*, the coil-to-globule transition of grafted PNIPAAm chains is classified as the true second order thermodynamic phase transition.[19,20]

It has been well established in numerous theoretical,[21–25] computational[26–32] and experimental[33–35] studies that the properties and behavior of the grafted polymer chains are dictated by the grafting density as well as the molecular weight of the polymer chains. The mushroom conformation is characteristic of not too densely grafted short chains. On the other hand, the lateral repulsion makes the densely grafted chains to adopt a brush conformation. The effect of grafting density was explored using atomic force microscopy and quartz crystal microbalance techniques.[36] While the conformational changes of grafted PNIPAAm chains became less abrupt with increasing grafting density, these changes start at lower temperatures, well below the LCST of free PNIPAAm chains. The influence of both the grafting density and the molecular weight of PNIPAAm chains on the temperature induced conformational transition was reported by Plunkett and co-workers.[37] Based on the contact angle measurements, the authors concluded that the temperature induced conformational changes became apparent at sufficiently high grafting density and higher molecular weights.

Since PNIPAAm is an amphiphilic polymer, the coil-to-globule transition is due to the interplay of hydrophobic and hydrophilic factors. It has been shown that PNIPAAm chains contain hydrophobic and hydrophilic domains; above the LCST the PNIPAAm chains are not completely hydrophobic, similarly they are not completely hydrophilic below the LCST.[38] Several authors pointed out abrupt changes in the contact angle measured on the layer of PNIPAAm chains grafted onto supporting substrates.[18,39,40] The values of the contact angle reflect only the degree of hydration in the uppermost layer of the grafted chains, whereas the process of dehydration starts in the inner layers.[17] However, the dynamics of water droplets on the grafted PNIPAAm chains, particularly using molecular simulations, is still not investigated. Moreover, the behavior of water within the PNIPAAm brush such as the formation of hydrogen bonds and their role in the contact angle of a water droplet on the brush layer is not well characterized under different state conditions.

In this work, molecular dynamics (MD) simulations are performed to study the contact angle of a water droplet on the end-grafted layer of thermo-responsive PNIPAAm polymer brushes over the temperature range covering the LCST of free PNIPAAm chains in water solution. The present study is focused on the structural properties of the monodisperse layer of grafted PNIPAAm chains, the interactions of PNIPAAm chains with water molecules and the dynamics of water molecules in order to explain the phase transition of PNIPAAm chains and the evolution of the water contact angle on the grafted PNIPAAm layer. Although there is an MD study concerning the thermal deswelling process of PNIPAAm brushes,[41] to the best of our knowledge, the present work is the first to report the contact angles of water molecules on the interface of the PNIPAAm brush at different temperatures using all-atom MD simulations.

2. Model and methodology

In this work, the interactions between grafted PNIPAAm chains and water molecules are simulated employing a fully flexible atomistic MD model. The PNIPAAm chains consisting of 30 *N*-isopropylacrylamide monomer units are anchored to a silicon substrate. As mentioned in the previous section, the grafting density substantially affects the phase transition of the grafted polymers. Lee *et al.* reported, in their recent work, that the packing energy of PNIPAAm on the silicon surface reaches a minimum at an area per chain of 1.1493 nm^2 per chain,[41] which is also considered in the present work. The supporting silicon (111) substrate is aligned with the x and y axes in the Cartesian coordinate system. The parameters of the orthorhombic simulation lattice were a = 11.972 nm, b = 3.456 nm and c = 20 nm. The initial conformation of a simulated system is built up of 36 (12 × 3) straight PNIPAAm chains placed perpendicular to the silicon surface (along the z axis). The terminal atom of each PNIPAAm chain is immobilized, *i.e.* it is kept frozen at the C–Si equilibrium distance above the silicon surface. Although the silicon atoms are kept frozen during the simulations, they are allowed to interact with the PNIPAAm chains and water molecules.

The intra- and intermolecular interactions between atoms are described by the OPLS force field,[42] and the SPCE model[43] was used for water molecules. Though the combination of the SPCE water model and the OPLS-AA force field is not typical, Walter *et al.* have shown that this combination predicts the temperature induced swelling and deswelling for PNIPAAm chains in water.[44] The long range Coulombic interaction is calculated using the Ewald summation technique. The bond lengths and angles in water molecules are held fixed using the SHAKE algorithm.[45] The position of the Gibbs interface of PNIPAAm chains is determined using the hyperbolic tangent function of the following form:

$$\rho = \frac{1}{2}(\rho_l + \rho_v) + \frac{1}{2}(\rho_l - \rho_v)\tanh\left(\frac{2(z - zl)}{\delta}\right), \qquad (1)$$

 This journal is © The Royal Society of Chemistry 2016

Published on 28 January 2016. Downloaded by Indian Institute of Technology Kanpur on 9/24/2021 8:03:59 AM.

with ρ_l being the density of polymer chains, ρ_v the density of water vapor, z the height of the grafted layer from the supporting surface, zl the height of the interface of the PNIPAAm layer from the surface and δ the width of the interface; for polymers, $\rho_v = 0$. Eqn (1) is used for the calculation of the liquid–vapor interfacial location of water above the polymer. In order to obtain the end points of the droplet, defining the vapor–liquid interface is necessary for the calculations of the contact angle. The contact angles were obtained from the slope to the fitted end points of the droplet.[46]

The average height of the PNIPAAm layer is evaluated from the normalized first moment of the monomer density distribution along the surface normal:

$$h_{av} = \frac{\int_0^\infty z\rho(z)\mathrm{d}z}{\int_0^\infty \rho(z)\mathrm{d}z}. \quad (2)$$

Hydrogen bonds between the carboxyl oxygen O_p of PNIPAAm and the water hydrogen H_w satisfy the geometric criteria due to Luzar and Chandler:[47] $r_{O_p\text{–}O_w} \leq 3.60$ Å, $r_{O_p\text{–}H_w} \leq 2.45$ Å and $\theta_{O_p\text{–}O_w\text{–}H_w} \leq 30^\circ$, where $r_{O_p\text{–}O_w}$ and $r_{O_p\text{–}H_w}$ are the distances and $\theta_{O_p\text{–}O_w\text{–}H_w}$ is the angle between the respective atoms. The potential of mean force (PMF) is estimated from the relation $U_{PMF} = -k_BT\ln[g(r)]$, where k_B is the Boltzmann constant, T is the absolute temperature and $g(r)$ is the radial distribution function.

The lateral and perpendicular components of the diffusion coefficient of water molecules are evaluated from the mean-square displacements as follows:

$$D_{xy} = \frac{1}{4}\lim_{t\to\infty}\frac{\mathrm{d}}{\mathrm{d}t}\left\langle (x(t+\mathrm{d}t) - x(t))^2 + (y(t+\mathrm{d}t) - y(t))^2\right\rangle, \quad (3)$$

$$D_z = \frac{1}{2}\lim_{t\to\infty}\frac{\mathrm{d}}{\mathrm{d}t}\left\langle (z(t+\mathrm{d}t) - z(t))^2\right\rangle \quad (4)$$

where $x(t)$, $y(t)$, and $z(t)$ are the position vector components of a water molecule at time t. The averages run over all analyzed conformations and different initial times dt.

One needs to keep in mind that the kinetics of such high-density systems is slow and it is necessary to verify whether the equilibrium has been achieved during the MD simulations. The relaxation times of PNIPAAm chains obtained from the end-to-end distance autocorrelation functions and the time evolution of a water droplet are used as the gauges of the equilibrium of the presented systems. Both quantities confirm the system equilibrium. The temperature is more precisely controlled in the experimental measurements with the fluctuations being of the order of ± 0.1 °C[18,48] than in the simulations where the temperature fluctuations are about ± 1.5 °C.

3. Simulation details

Since the periodic boundary conditions were imposed in all directions, the box height of 20 nm in the perpendicular direction was found to be long enough to prevent the PNIPAAm chains from the interactions with the opposite surface. Because the hydration of PNIPAAm brushes using the MD method was time demanding the grand canonical Monte Carlo (GCMC) technique was implemented to hydrate the brush. Initially 200 water molecules were inserted randomly into the grafted PNIPAAm layer. Subsequently, at every 1.0 ps, 10 000 attempts were made for insertion/deletion, rotation and translation of water molecules with probabilities of 0.5, 0.25 and 0.25, respectively, at 300 K. The saturation of the PNIPAAm brush was achieved with 3530 ± 20 water molecules, which comprises a weight percentage of $\sim$35% at 300 K. The experimentally reported amount of water inserted into the PNIPAAm brush is about 45% at 23 °C.[49] This is slightly higher water uptake than the content achieved by the GCMC method. It might be accounted for by a lower grafting density, although not reported in the experimental study, and the lower temperature used in the experiment. After hydration, the initial system was allowed to equilibrate using the MD technique for 20 ns independently at different temperatures, ranging from 270 K to 340 K, with a temperature increment of 10 K.

A cylinder of water containing 2000 molecules, with a diameter of $\sim$2.0 nm and length equal to the width of the grafted PNIPAAm system, was equilibrated in an *NVT* ensemble for 2.0 ns at 300 K. The cylindrical shape of the water droplet was chosen to reduce the effect of line tension. The equilibrated water cylinder was placed in the close vicinity of the equilibrated hydrated PNIPAAm layer as shown in Fig. 1a. The systems after 25 ns of MD simulations at different temperatures in the *NVT* ensemble are shown in Fig. 1b–e. The systems were sampled at a time interval of 10.0 ps, and the properties of the systems, such as the end-to-end distance, the contact angle of the water droplet, and hydrogen bonding, were calculated as the ensemble averages of the last 2 ns. The density profiles were evaluated over the last 2.0 ns and the radial distribution functions were calculated over the last 1.0 ns.

All simulations were carried out using the LAMMPS package.[50] The PPPM (Particle-Particle–Particle-Mesh) technique[51] was used for the calculations of the long-range electrostatic interactions with a cut-off distance of 1.0 nm. The cut-off for the Lennard-Jones potential was kept at 1 nm. A Nosé–Hoover thermostat was used to maintain the temperature constant during the simulations with a relaxation time of 0.1 ps. The integration time step was set to 1.0 fs.

4. Results and discussion

Fig. 2 shows the density profile of water and PNIPAAm chains along the normal to the surface at a temperature of 270 K. In order to evaluate the contact angle of water molecules on the top of the PNIPAAm brush, the interface between the brush and water needs to be defined. Eqn (1) is used to determine the position of the interface of the PNIPAAm layer. This interface is also included in Fig. 2. The average monomer density is $\sim$0.78 g cm^{-3}. The density of water within the PNIPAAM chains, $\sim$0.375 g cm^{-3}, is significantly lower than the bulk liquid density. However, it swiftly increases across the interface to the bulk value. The density of water sharply decreases to the

Published on 28 January 2016. Downloaded by Indian Institute of Technology Kanpur on 9/24/2021 8:03:59 AM.

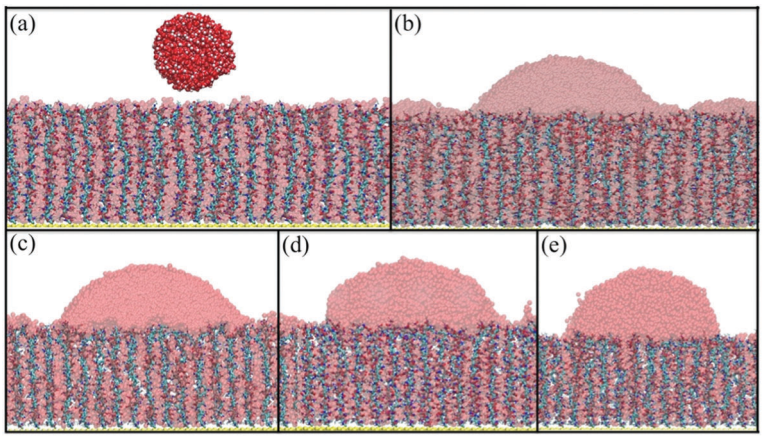

Fig. 1 Snapshots of the initial structure of the system when a cylindrical water droplet is placed close to the hydrated PNIPAAm layer (a) and of the water droplet morphologies shown at temperatures 270 K (b), 300 K (c), 310 K (d) and 320 K (e) after 25 ns.

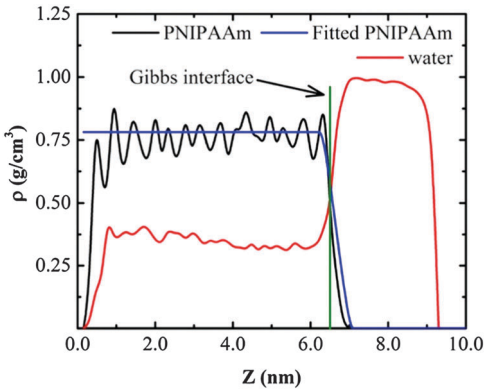

Fig. 2 Density profile of PNIPAAm chains and water along the normal of the silicon surface at 270 K. Polymer and water densities are represented by black and red lines, respectively. The blue line shows the overall polymer density to determine the Gibbs interface (green line).

value of the vapor density with a further increase in the distance from the interface.

The density profiles of PNIPAAm chains and water molecules at different temperatures are shown in Fig. 3a. The oscillatory behavior of the density profiles indicates a rather rigid conformation of the stretched densely grafted PNIPAAm chains. However, the positional ordering of PNIPAAm chains in the close vicinity of the surface does not display any enhanced amplitudes. It follows that there are no significant attractive interactions between the grafted amphiphilic PNIPAAm chains and the non-polar silicon substrate. Thus, only oscillations around the average value of density are observed over the whole density profile. The shape of the density profiles of PNIPAAm is far from being parabolic with the maximum at the surface boundary as predicted theoretically for a polymer brush in a good solvent.[24] The shape is step-like already at lower temperatures. This is typical for densely grafted polymer brushes in poor-solvent or dry conditions.[19] As can be inferred from the vanishing of the density profiles in Fig. 3a the Gibbs interface is shifted closer to the silicon surface with increasing temperature. Nevertheless, this effect is not very significant (Fig. 3b). Interestingly, the shift in the interface position is linearly dependent on the temperature. Experimental data from Balamurugan *et al.* also show a linear dependence of the layer thickness on temperature in the middle of the temperature regime.[16] The decline of the distance of the Gibbs interface from the silicon substrate induced by an increase in temperature for relatively short PNIPAAm chains agrees well with the experimental findings.[37]

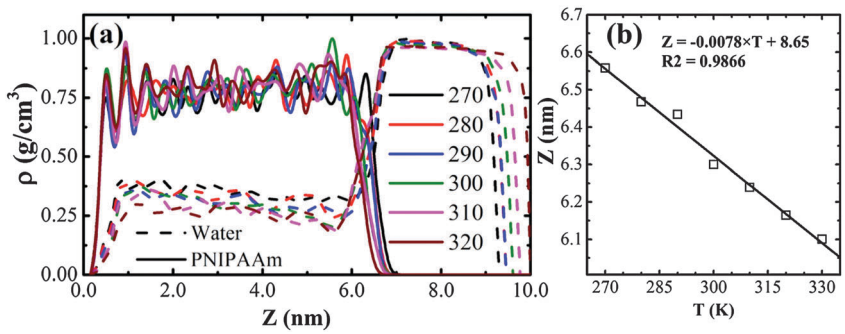

Fig. 3 Density profile of PNIPAAm chains and water along the normal of the silicon surface at different temperatures (a). Solid and dashed colored lines are used to discern the density of PNIPAAm and water, respectively. (b) The position of the Gibbs interface as a function of temperature after 25.0 ns.

 This journal is © The Royal Society of Chemistry 2016

Published on 28 January 2016. Downloaded by Indian Institute of Technology Kanpur on 9/24/2021 8:03:59 AM.

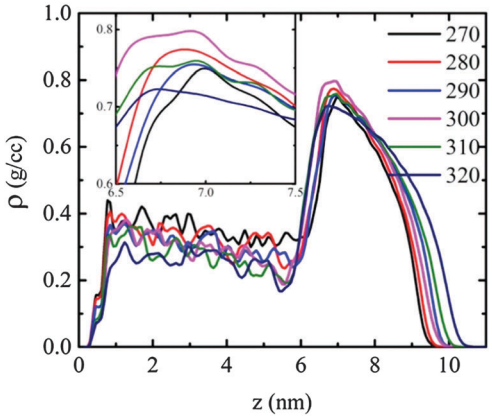

Fig. 4 Cross-sectional water density profile along the surface normal (*z* axis) at different temperatures. The inset shows a zoom-in view of the water density profile above the interface.

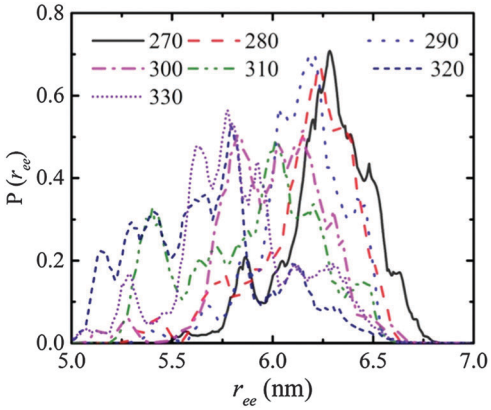

Fig. 5 Variation of the probability distribution of the end-to-end distance of PNIPAAm chains with temperature.

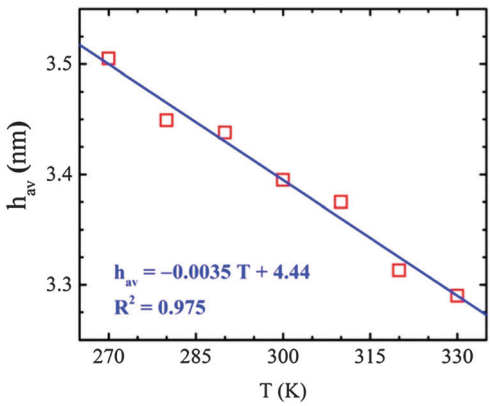

Fig. 6 Variation of the normalized first moment of the monomer density distribution as a measure of the average height of grafted PNIPAAm chains with temperature.

The decrease of water density inside the PNIPAAm brush and the increased amount of water outside the PNIPAAm brush with increasing temperature suggest the accumulation of water molecules at the interface. This indicates the reorganization of PNIPAAm chains and their propensity to collapse as the temperature increases. The water expulsion from the grafted PNIPAAm layer is more evident in the total cross-sectional density profile of water as shown in Fig. 4, which, in addition, renders the qualitative notion of the shape of a water droplet. The extension of the water droplet and hence the area under the curve of water–density profiles correlates with the temperature induced accumulation of water molecules. In fact, the shrinking of the PNIPAAm layer results from the expulsion of water molecules. Nevertheless, although the process of expulsion is very slow, as also seen by Lee *et al.*,[41] the time evolution of the water contact angle and the autocorrelation function of the end-to-end distance confirm the equilibration of the presented systems. It has been shown that the local water density fluctuations evaluated using the INDUS algorithm developed by Patel *et al.*[52,53] represent a suitable way of characterizing the interfacial water and the nature of interaction (hydrophobic or hydrophilic) with the underlying substrate. The absence of layering in the water density profiles near the surface, in the current work, suggests that the simple density profile may not be sufficient to characterize the degree of hydrophobicity of the polymer brush.[54] Though the study of local water density fluctuations is beyond the focus of the current work, it will be undertaken to address the thermo-responsive systems in the future.

In order to provide more quantitative insight into the response of grafted PNIPAAm chains to temperature changes, the end-to-end distance r_{ee} (the distance of the free terminal monomer from the grafted atom) and the average height of PNIPAAm chains at different temperatures are calculated. The influence of the temperature on the probability distribution of the end-to-end distance $P(r_{ee})$ of PNIPAAm chains is displayed in Fig. 5. Upon increasing the temperature, the peak of $P(r_{ee})$ is shifted towards lower values of r_{ee} and the probability distribution is also broadened. Such a variation is consistent with the collapse of PNIPAAm chains when the free terminal monomer penetrates the grafted layer in the process of compaction of the PNIPAAm layer.

The normalized first moment of the monomer density distribution (see eqn (2)) as a measure of the average height of the polymer layer shown in Fig. 6 monotonically decreases with increasing temperature. This is expected from the temperature dependence of the density distributions, the position of the Gibbs interface of the PNIPAAm layer (Fig. 3) and probability distributions of the end-to-end distance of PNIPAAm chains (Fig. 5). Nevertheless, the change in the height of the PNIPAAm layer in the temperature range of 270–330 K is only marginal (6%).

As the temperature changes do not cause significant modification in the conformation of relatively short PNIPAAm chains densely grafted onto the silicon substrate, the interest is in the respective response of the water contact angle. The contact angle of water measured on the interface of grafted PNIPAAm chains is found to change abruptly at the LCST.[16,18,40] The measurement of the contact angle on these kinds of surfaces is challenging due to their inherent soft interface. The Gibbs interface of the PNIPAAm layer is considered in the calculations of the contact angle of a water droplet. Since there is no

Published on 28 January 2016. Downloaded by Indian Institute of Technology Kanpur on 9/24/2021 8:03:59 AM.

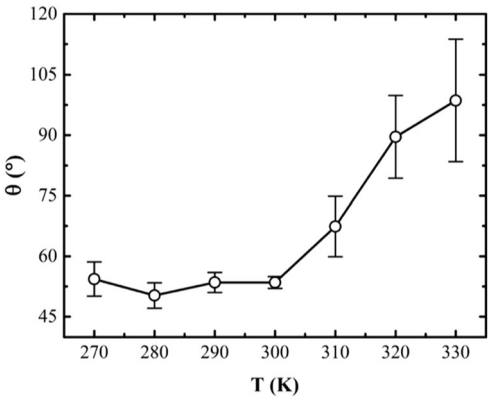

Fig. 7 Variation of the contact angle of a water droplet on the PNIPAAm brush with temperature. The line serves as guide to the eye.

discontinuity in the density profile of water across the PNIPAAm–water interface, the Gibbs interface is considered as a baseline for the calculations of the contact angle. Fig. 7 shows the variation of the water contact angle with temperature. Snapshots of the droplet at different temperatures are shown in Fig. 1b–e. At temperatures below the LCST, the values of the water contact angle on the PNIPAAm interface remain more or less constant and oscillate in the range of 50°–60°. As the temperature rises above 300 K, the contact angle increases. At 330 K, the water contact angle reaches ~98°, a value characteristic of hydrophobic materials. However, higher temperatures are required for the plateau (not shown). Although the temperature induced variation of the contact angle is more substantial than the temperature induced conformational changes of the PNIPAAm layer, it is not as steep as it has been observed experimentally.[16,18,40] The experimentally measured values of advancing contact angles of water on the top of terminally grafted PNIPAAm chains increase gradually from ~50° to almost 90°, within the temperature range of ~3 °C (21–24 °C), as reported by Takei *et al.*[18] On the other hand, Balamurugan *et al.* have also reported a transition from 67° to about 78° with an increase in temperature from 31 °C to 32 °C.[16] The water contact angles observed in the current work using all-atom MD simulations are in good agreement with the reported experimental values.

The time evolution of the water contact angle at different temperatures is displayed in Fig. 8a. At lower temperatures (270–300 K) the contact angle remains virtually constant, at 310 K it saturates after about 10 ns, whereas the indication of saturation of the contact angle at 320 K and 330 K is observed after about 20 ns. These trends correlate well with the number of hydrogen bonds between the carboxyl oxygen of PNIPAAm chains and water molecules evaluated per carboxyl oxygen (Fig. 8b).

It is generally accepted that the change in the hydrogen bonding network between PNIPAAm chains and water molecules resulting from the temperature variation mostly governs the temperature induced conformational transition of PNIPAAm chains. Three types of hydrogen bonds are feasible for PNIPAAm chains in water: PNIPAAm–PNIPAAm pair (N–H···O=C) and PNIPAAm–water (N–H···O–H and O–H···O=C). One should notice here that the hydrogen bonds between water hydrogen and carboxyl oxygen (O–H···O=C) prevail[9] and also possess the longest relaxation time.[15] Fig. 9a shows the temperature dependence of the number of hydrogen bonds between PNIPAAm chains and water molecules evaluated per carboxyl oxygen atom. With increasing temperature, the number of hydrogen bonds between the water and the carboxyl group as well as between water molecules inserted in the PNIPAAm layer (Fig. 9b) monotonically decreases in agreement with the increasing contact angle, which is in line with the analysis of Lee *et al.*[41] The time dependence of the number of hydrogen bonds between the carboxyl oxygen of PNIPAAm chains and water molecules evaluated per carboxyl oxygen (Fig. 8b) also correlates well with the time dependence of the water contact angle, *i.e.*, at higher temperatures, the variation of the number of hydrogen bonds becomes more significant. For comparison, the number of water–water hydrogen bonds per one water molecule in the bulk water has also been calculated. Upon increasing the temperature from 270 K to 330 K, this number drops from 3.7 to 3.5, consistent with other simulation studies using the SPCE water model.[55,56] Though, in the PNIPAAm layer, the number of hydrogen bonds between water molecules is reduced, the interval width of the variation stays similar to the interval width for bulk water.

Temperature influences the diffusion of water molecules confined in the grafted PNIPAAM layer directly and also indirectly through the modification of the hydrogen bond network.

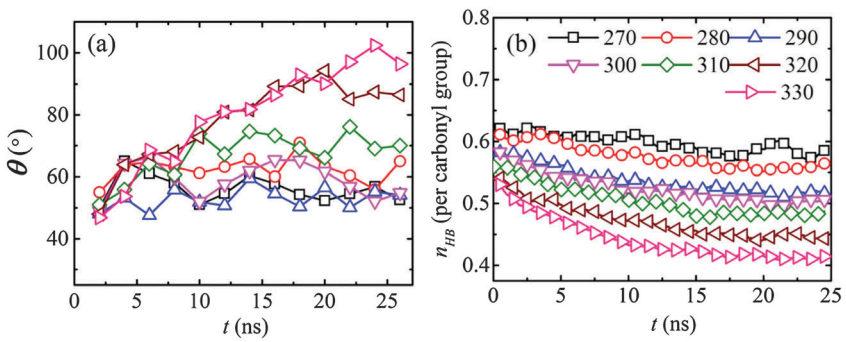

Fig. 8 Time evolution of the water contact angle (a) and the number of hydrogen bonds between the carboxyl oxygen of PNIPAAm chains and water molecules evaluated per carboxyl oxygen (b) at different temperatures.

 This journal is © The Royal Society of Chemistry 2016

Published on 28 January 2016. Downloaded by Indian Institute of Technology Kanpur on 9/24/2021 8:03:59 AM.

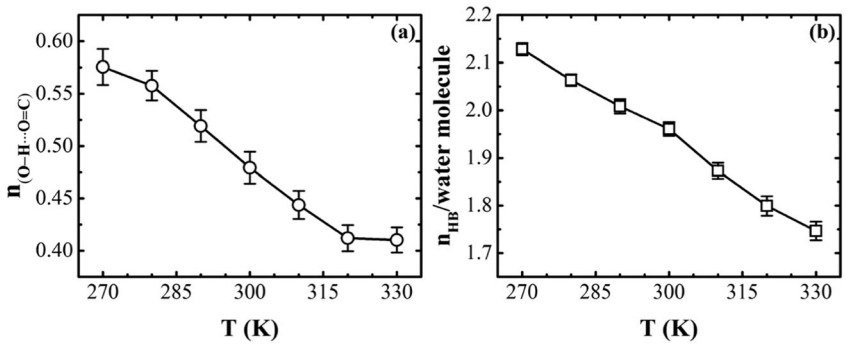

Fig. 9 Variation of the average number of hydrogen bonds between the carboxyl oxygen of PNIPAAm chains and water molecules evaluated per one carboxyl oxygen (a), and of the average number of hydrogen bonds between water molecules inserted in the PNIPAAm layer per water molecule (b) with temperature. The corresponding number of hydrogen bonds between water molecules in bulk water decreases from 3.7 to 3.5 in the investigated temperature interval. The lines serve as guide to the eye.

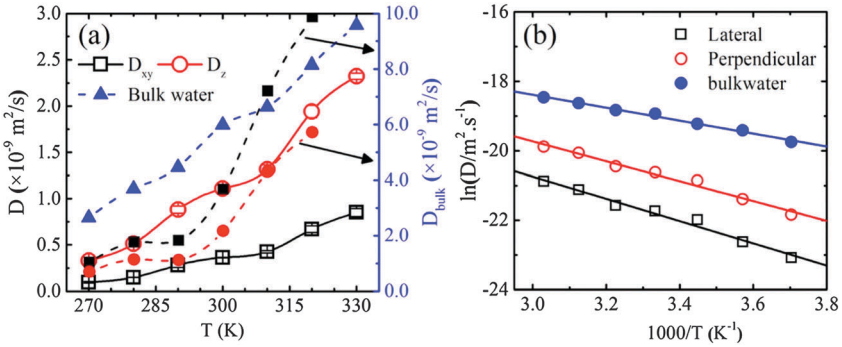

Fig. 10 Temperature dependence of the lateral (black squares) and perpendicular (red circles) components of the diffusion coefficient of water molecules inserted in the relaxed (open symbols) and stretched (solid symbols) PNIPAAm layer (a). The corresponding Arrhenius plots (b). The left axis shows the scale for the lateral and perpendicular diffusion components of the relaxed PNIPAAm layer, whereas the right axis shows the scale for that of stretched chains and bulk diffusion (solid blue triangles). All lines serve as guide to the eye.

The PNIPAAm layer represents an anisotropic environment for water molecules. This is evident in Fig. 10a, which shows the temperature dependence of the lateral and perpendicular components (with respect to the silicon surface) of the diffusion coefficients of water molecules inside the PNIPAAm brushes. The plot of the respective bulk water diffusion coefficients is also shown. The diffusion of water molecules inserted in the PNIPAAm layer is significantly lower than the self-diffusion of bulk water molecules. While at low temperature, 270 K, the lateral and perpendicular components are almost the same, the lateral diffusion of water molecules is reduced compared to the perpendicular diffusion with increasing temperature as anticipated for water molecules leaving a grafted polymer layer. The perpendicular diffusion of water molecules becomes twice the lateral water diffusion at 330 K. At higher temperature, water molecules move more easily in the perpendicular direction. This is not surprising since no entanglement is expected in the collapsed state of PNIPAAm chains with such a short chain length. The activation energy obtained from the Arrhenius plots (Fig. 10b) is 6.373 ± 0.384 kcal mol^{-1} for the lateral diffusion of water molecules, 5.695 ± 0.337 kcal mol^{-1} for the perpendicular diffusion of water molecules, and 3.710 ± 0.153 kcal mol^{-1} for the self-diffusion of water molecules in the bulk, which is, however, in good agreement with experimental values of 4.4–4.8 kcal mol^{-1} and other simulation values.[8] In order to address the influence of the coiled or collapsed conformation of PNIPAAm chains on the anisotropy of water diffusion, the MD simulations with PNIPAAm chains stretched along the surface normal were performed. The results are included in Fig. 10a. The chains were stretched to their geometric length by applying a force on the topmost monomers and restrained them using a spring to the fixed height. The rest of the monomers were kept unrestrained. As seen in Fig. 10a, the diffusion coefficients of water molecules in the restrained polymer brush, though higher than those observed for the relaxed layer of PNIPAAm chains, are lower than those in the bulk water. Interestingly, the diffusion coefficient in the perpendicular direction is smaller than in the lateral direction which might be attributed to the influence of the substrate. Since now the potential gradient arising from the substrate is not shielded so efficiently by stretched PNIPAAm chains as in the case of the relaxed PNIPAAm chains the water molecules have to overcome the ensuing potential gradient.

In addition to the water diffusion, the reorganization of grafted PNIPAAm chains is also reflected in the PNIPAAm–water structural properties. The radial distribution functions of polymer–water and water–water pairs are shown in Fig. 11a and b,

Published on 28 January 2016. Downloaded by Indian Institute of Technology Kanpur on 9/24/2021 8:03:59 AM.

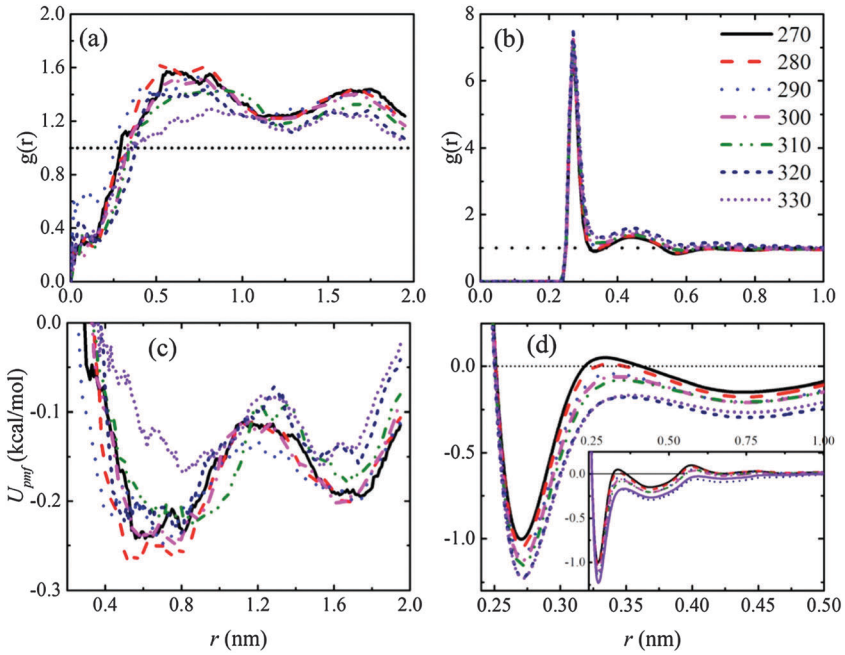

Fig. 11 Radial distribution functions of PNIPAAm–water pair (a) and water–water pair (b) interactions. The potential of mean force of PNIPAAm–water pair and water–water pair interactions is shown in panels (c) and (d), respectively. The PMF of water–water pair interactions till the cut-off distance is shown in the inset of panel (d).

respectively. The PNIPAAm–water RDF, calculated based on the center of mass of polymer chains with water molecules, is clearly affected by the temperature. The position of the peaks does not change significantly with increasing temperature. However, the intensity of the first two peaks decreases significantly with the increase in temperature. This clearly indicates that the number of water molecules around a PNIPAAm chain decreases with increasing temperature. Furthermore, the trend of the intensity of both peaks, induced by the changes in temperature, suggests that the water molecules in both coordination shells tend to leave the PNIPAAm brush simultaneously. The reverse trend is observed for the water–water pair interaction, where the second hydration shell increases with increasing temperature while the first hydration shell is virtually unaffected by temperature. The above behavior indicates the expulsion of water from the brush moiety. What would be the governing factor in the process of expulsion of water from the brush moiety? In order to address this question, the PMFs of PNIPAAm–water and water–water pairs at different temperatures have been calculated and are shown in Fig. 11c and d, respectively. The PMF of PNIPAAm–water increases with increasing temperature, as shown in Fig. 11c. At higher temperatures, the energy barrier is lower compared to that at lower temperatures. On the other hand, Fig. 11d indicates the lowering of the PMF value of water–water with increasing temperature. This clearly indicates a decrease in water–polymer affinity with increasing temperature, leading to expulsion of water from the brush moiety at higher temperature. Thus the PMF plots are in line with the notion that the water molecules tend to be expelled from the PNIPAAm chains. However, the overall change in the free energy is negative with the increase in temperature which agrees with more rigorous calculations carried out by Lee *et al.*[41]

The "two-body" contribution to the excess entropy, shown in Fig. 12a, which describes the translational order, was calculated from the radial distribution function for PNIPAAm–water pair and water–water pair interactions as follows:[57]

$$S_{ij} = -2\pi\rho k_B \int \left[g_{ij}(r)\ln g_{ij}(r) - g_{ij}(r) + 1\right] r^2 \mathrm{d}r, \qquad (5)$$

where ρ is the number density of the system and indices i and j denote the interacting centers. The excess entropy resulting from the PNIPAAm–water binary interaction monotonically increases whereas that of water–water interaction decreases with increasing temperature. This is expected since the number of PNPAAm–water hydrogen bonds decreases, which leads to the increased number of degrees of freedom. The excess entropy is found negative here. Though the enthalpy of coil-to-globule transition appeared to be positive, the entropy gain ascribed to the larger volume available for water molecules and their release from monomer–water hydrogen bonds at higher temperatures prevailed.[13]

The second virial coefficient, B_2, has been calculated from the PMF functions as $B_2 = -\frac{1}{2}\int_0^\infty [\exp(-\beta U_{\mathrm{PMF}}(r)) - 1] 4\pi r^2 \mathrm{d}r$. B_2 reflects the binary interactions and depends on the potential energy between interacting particles. The favorable binary interactions leading to the attraction are characterized by $B_2 < 0$ (or decreasing trend), whereas $B_2 > 0$ (or increasing trend) indicates the repulsive binary interactions. Hence, B_2 values and its behavior can be used to identify the tendency of the system to agglomerate or disperse. This has been effectively used to quantify the agglomeration/dispersion behavior of

 This journal is © The Royal Society of Chemistry 2016

Published on 28 January 2016. Downloaded by Indian Institute of Technology Kanpur on 9/24/2021 8:03:59 AM.

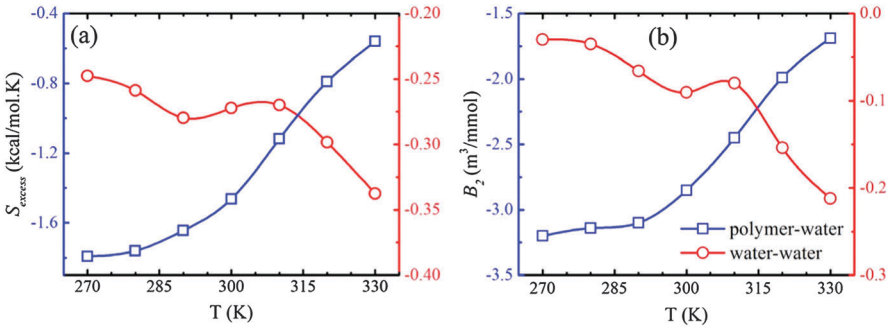

Fig. 12 Temperature dependence of the excess entropy S_{excess} (a) and the second virial coefficient B_2 (b). The left and right ordinates are associated with PNIPAAm–water pairs (blue squares) and water–water pairs (red squares), respectively. All lines serve as guide to the eye.

nanoparticles in a polymer matrix in our recent studies.[58,59] Fig. 12b shows the temperature dependence of B_2 for PNIPAAm–water and water–water interactions. Here, B_2 of the PNIPAAm–water pair increases with increasing temperature, while B_2 of the water–water pair tends to decrease with increasing temperature. This essentially indicates that water molecules prefer to be expelled from the brush moiety with increasing temperature. This is further strengthened by the behavior of B_2 of water–water, which shows a decreasing trend with increasing temperature, indicating the growing attraction between the water molecules (*i.e.*, lowering of PMF values as also seen in Fig. 11d). At lower temperatures, the PNIPAAm chains remain hydrated, which is evident from the hydrogen bonding analysis as well as the PNIPAAm–water RDF, and hence PNIPAAm chains adopt a swollen conformation which is deduced from the end-to-end distribution (see Fig. 5). As the temperature increases, the end-to-end profile indicates shrinking, *i.e.* collapse of PNIPAAm chains. From Fig. 12, it follows that the entropy effects, associated with the release of water molecules from the PNIPAAm brush at elevated temperatures, dominate the coil-to-globule transition. On the other hand, the water–water pair contributes to the temperature induced dehydration of PNIPAAm brushes enthalpically.

5. Conclusion

In this work, all-atom MD simulations have been employed to study the wetting transition of water on a densely grafted silicon surface with PNIPAAm chains. Furthermore, conformation transitions of hydrated thermo-responsive PNIPAAm chains are also studied. The collapse of relatively short PNIPAAm chains (30 monomer units) induced by an increase in temperature above the LCST is observed in the density profiles of PNIPAAm chains and water (along the normal of the surface), probability distributions of the end-to-end distances of PNIPAAm chains, the height of the grafted PNIPAAm layer, the shift in the position of the Gibbs interface of the grafted PNIPAAm layer and water contact angle measurements. The temperature induced structural changes are less significant than the corresponding changes in the water contact angle. The increase of the contact angle with increasing temperature is significant despite the low molecular weight of investigated PNIPAAm chains, which is most likely attributable to the high grafting density of PNIPAAm chains. The analysis of hydrogen bonds between PNIPAAm chains and water molecules, radial distribution functions and the potential of mean force indicate that the PNIPAAm–water interactions play a more important role in the coil-to-globule transition. The increase in excess entropy clearly indicates the propensity for dehydration of PNIPAAm chains with increasing temperature, suggesting that the coil-to-globule transition is mainly an entropy driven process.

Acknowledgements

This work was supported by the Department of Science & Technology, Govt. of India, and European Science and Technology Council. This work is part of Indo-Portugal Collaboration funded by International Division of DST, Government of India (INT/PORTUGAL/P-05/2013). Thanks are also due to the Portuguese Fundação para a Ciência e Tecnologia (FCT, Lisbon) and to FEDER for financial support to LAQV@REQUIMTE, Project UID/QUI/50006/2013, as well as to grants SRDA-0451-11, VEGA 2/0098/16 and VEGA 2/0055/16. This work was also partially supported by the Indo-Portuguese Programme of Cooperation in Science and Technology. Z. B. further acknowledges FCT for the postdoctoral grant SFRH-BPD-90265-2012 co-financed by the European Social Fund. The authors are greatly indebted to all financing sources, as well as to the HPC Centre, IIT Kanpur for providing the computational facility.

References

1 H. Kuroki, I. Tokarev and S. Minko, *Annu. Rev. Mater. Res.*, 2012, **42**, 343–372.
2 M. A. Cole, N. H. Voelcker, H. Thissen and H. J. Griesser, *Biomaterials*, 2009, **30**, 1827–1850.
3 E. Kharlampieva, V. Kozlovskaya, J. Tyutina and S. A. Sukhishvili, *Macromolecules*, 2005, **38**, 10523–10531.
4 A. Chundera, K. Etcheverryb, G. Londec, H. J. Chob and L. Zhai, *Colloids Surf., A*, 2009, **333**, 187–193.
5 B. C.-K. Tee, C. Wang, R. Allen and Z. Bao, *Nat. Nanotechnol.*, 2012, **7**, 825–832.

Published on 28 January 2016. Downloaded by Indian Institute of Technology Kanpur on 9/24/2021 8:03:59 AM.

6 Y. Chen, A. M. Kushner, G. A. Williams and Z. Guan, *Nat. Chem.*, 2012, **4**, 467–472.
7 L. Zhai, *Chem. Soc. Rev.*, 2013, **42**, 7148–7160.
8 Y. Tamai, H. Tanaka and K. Nakanishi, *Macromolecules*, 1996, **29**, 6761–6769.
9 Y. Tamai, H. Tanaka and K. Nakanishi, *Macromolecules*, 1996, **29**, 6750–6760.
10 B. M. Baysal and F. E. Karasz, *Macromol. Theory Simul.*, 2003, **12**, 627–646.
11 P. A. Netz and T. Dorfmüller, *J. Phys. Chem. B*, 1998, **102**, 4875–4886.
12 G. Longhi, F. Lebon, S. Abbate and S. L. Fornili, *Chem. Phys. Lett.*, 2004, **386**, 123–127.
13 G. Graziano, *Int. J. Biol. Macromol.*, 2000, **27**, 89–97.
14 T. Tönsing and C. Oldiges, *Phys. Chem. Chem. Phys.*, 2001, **3**, 5542–5549.
15 S. Deshmukh, D. A. Mooney, T. McDermott, S. Kulkarni and J. M. D. MacElroy, *Soft Matter*, 2009, **5**, 1514–1521.
16 S. Balamurugan, S. Mendez, S. S. Balamurugan, M. J. O'Brien-II and G. P. López, *Langmuir*, 2003, **19**, 2545–2549.
17 H. Yim, M. S. Kent, S. Satija, S. Mendez, S. S. Balamurugan, S. Balamurugan and G. P. López, *Phys. Rev. E: Stat., Nonlinear, Soft Matter Phys.*, 2005, **72**, 051801.
18 Y. G. Takei, T. Aoki, K. Sanui, N. Ogata, Y. Sakurai and T. Okano, *Macromolecules*, 1994, **27**, 6163–6166.
19 E. B. Zhulina, V. Borisov, V. A. Pryamitsyn and T. M. Birshtein, *Macromolecules*, 1991, **24**, 140–149.
20 X. Laloyaux, B. Mathy, B. Nysten and A. M. Jonas, *Langmuir*, 2010, **26**, 838–847.
21 S. Alexander, *J. Phys.*, 1977, **38**, 983–987.
22 P. G. d. Gennes, *Macromolecules*, 1980, **13**, 1069–1075.
23 S. T. Milner, T. A. Witten and M. E. Cates, *Macromolecules*, 1988, **21**, 2610–2619.
24 S. T. Milner, T. A. Witten and M. E. Cates, *Europhys. Lett.*, 1988, **5**, 413–418.
25 S. T. Milner, *Science*, 1991, **251**, 905–914.
26 M. Murat and G. S. Grest, *Macromolecules*, 1989, **22**, 4054–4059.
27 P. Y. Lai and K. Binder, *J. Chem. Phys.*, 1991, **95**, 9288–9299.
28 P. Y. Lai and K. Binder, *J. Chem. Phys.*, 1992, **97**, 586–595.
29 A. Chakrabarti, *J. Chem. Phys.*, 1994, **100**, 631–635.
30 D. Bedrov and G. D. Smith, *Langmuir*, 2006, **22**, 6189–6194.
31 Z. Benková and M. N. D. S. Cordeiro, *J. Phys. Chem. C*, 2012, **116**, 3576–3584.
32 F. Goujon, C. Bonal, B. Limoges and P. Malfreyt, *J. Phys. Chem. B*, 2008, **112**, 14221–14229.
33 P. Auroy, L. Auvray and L. Leger, *Macromolecules*, 1991, **24**, 2523–2528.
34 J. Piehler, A. Brecht, R. Valiokas, B. Liedberg and G. Gauglitz, *Biosens. Bioelectron.*, 2000, **15**, 473–481.
35 A. F. Miller, R. W. Richards and J. R. P. Webster, *Macromolecules*, 2001, **34**, 8361–8369.
36 N. Ishida and S. Biggs, *Macromolecules*, 2010, **43**, 7269–7276.
37 K. N. Plunkett, X. Zhu, J. S. Moore and D. E. Leckband, *Langmuir*, 2006, **22**, 4259–4266.
38 R. Pelton, *J. Colloid Interface Sci.*, 2010, **348**, 673–674.
39 R. Yoshida, K. Uchida, Y. Kaneko, K. Sakal, A. Kikuchi, Y. Sakurai and T. Okano, *Nature*, 1995, **374**, 240–242.
40 J. Zhang, R. Pelton and Y. Deng, *Langmuir*, 1995, **11**, 2301–2302.
41 S. G. Lee, T. A. Pascal, W. Koh, G. F. Brunello, W. A. Goddard-III and S. S. Jang, *J. Phys. Chem. C*, 2012, **116**, 15974–15985.
42 W. L. Jorgensen, D. S. Maxwell and J. Tirado Rives, *J. Am. Chem. Soc.*, 1996, **118**, 11225–11236.
43 H. J. C. Berendsen, J. R. Grigera and T. P. Straatsma, *J. Phys. Chem.*, 1987, **91**, 6269–6271.
44 J. Walter, V. Ermatchkov, J. Vrabec and H. Hasse, *Fluid Phase Equilib.*, 2010, **296**, 164–172.
45 J.-P. Ryckaert, G. Ciccotti and H. J. C. Berendsen, *J. Comput. Phys.*, 1977, **23**, 327–341.
46 A. K. Metya, S. Khan and J. K. Singh, *J. Phys. Chem. C*, 2014, **118**, 4113–4121.
47 A. Luzar and D. Chandler, *J. Chem. Phys.*, 1993, **98**, 8160–8173.
48 G. V. R. Rao, M. E. Krug, S. Balamurugan, H. Xu, Q. Xu and G. P. López, *Chem. Mater.*, 2002, **14**, 5075–5080.
49 J. J. Ramos and S. E. Moya, *Macromol. Rapid Commun.*, 2011, **32**, 1972–1978.
50 S. Plimpton, *J. Comput. Phys.*, 1995, **117**, 1–19.
51 B. A. Luty, I. G. Tironi and W. F. van-Gunsteren, *J. Chem. Phys.*, 1995, **103**, 3014–3021.
52 A. J. Patel, P. Varilly, D. Chandler and S. Garde, *J. Stat. Phys.*, 2011, **145**, 265–275.
53 A. J. Patel, P. Varilly and D. Chandler, *J. Phys. Chem. B*, 2010, **114**, 1632–1637.
54 R. Godawat, S. N. Jamadagni and S. Garde, *Proc. Natl. Acad. Sci. U. S. A.*, 2009, **16**, 15119–15124.
55 J. Zielkiewicz, *J. Chem. Phys.*, 2005, **123**, 104501.
56 C. Nieto-Draghi, J. Bonet Avalos and B. Rousseau, *J. Chem. Phys.*, 2003, **118**, 7954.
57 B. B. Laird and A. D. J. Haymet, *J. Chem. Phys.*, 1992, **97**, 2153–2155.
58 T. K. Patra and J. K. Singh, *J. Chem. Phys.*, 2013, **138**, 144901.
59 T. K. Patra and J. K. Singh, *Soft Matter*, 2014, **10**, 1823–1830.

 This journal is © The Royal Society of Chemistry 2016